Deep–Sea Research II xxx (xxxx) xxx

Contents lists available at ScienceDirect

Deep-Sea Research Part II

journal homepage: www.elsevier.com/locate/dsr2

An ocean perspective on CMIP6 climate model evaluations

A B S T R A C T

This paper serves as an introduction to the Deep-Sea Research II special issue entitled an ocean perspective on CMIP6 model evaluations, which reported the progress of CMIP6 (Coupled Model Intercomparison Project phase 6) emphasizing the ocean component. The six papers in this volume provided a series of evaluations, including ENSO (El Niño-Southern Oscillation) phase locking, Ningaloo Niño, global marine heat waves, freshwater flux-induced stratification over the central tropical Pacific, global sea levels, and AMOC (Atlantic meridional overturning circulation). To complement the papers in this volume and to present a general view of the performance of CMIP6 models in simulating sea surface temperature (SST) and sea surface salinity (SSS), the historical simulation biases from 48 and 46 CMIP6 models compared with observations are analyzed, respectively. Although not able to cover all the major aspects of model evaluation, this special issue has provided crucial information for model development and research based on climate models.

1. Introduction

The Coupled Model Intercomparison Project (CMIP) provides enormous datasets mainly produced by climate models for climate variability and change research. The latest (sixth) phase of CMIP (CMIP6) outputs has been published on the Earth System Grid Federation (ESGF). Therefore, it is necessary and urgent to evaluate the performances of CMIP6, how CMIP6 has made progress compared with previous generation models, and the projected climate change in the future. There are several journals such as Journal of Advances in Modeling Earth Systems, Geoscientific Model Development and Advances in Atmospheric Sciences, which provide special issues for the introduction and evaluation of CMIP6 datasets. This special issue, in particular, has solicited topics in climate variability and change evaluations of CMIP6 model simulations, which emphasize the ocean component.

To present a general picture of the performance of CMIP6 models in simulating sea surface temperature (SST) and sea surface salinity (SSS), the historical simulations of 48/46 models were chosen, as shown in Table 1, for SST/SSS comparison with observations. The climatology of SST is calculated between 1900 and 2014, and the observational reference dataset is the combination of HadISST (Rayner, 2003; https://www.metoffice.gov.uk/hadobs/hadisst/) and ERSST v5 (Huang et al., 2017, https://www.ncei.noaa.gov/pub/data/cmb/ersst/v5/netcdf/). The model bias of SSS is calculated during the period from 1955 to 2014 compared with the World Ocean Atlas 2018 (WOA18) dataset (Zweng et al., 2019, https://www.ncei.noaa.gov/products/world-ocean-atlas).

Fig. 1a–d shows the ensemble mean SST bias of four seasons from 48 models. The patterns of the bias are persistent throughout the annual cycle and thus the pattern of the annual mean SST bias (Fig. 1e) resembles the seasonal patterns. Compared with CMIP5 models (Wang et al., 2014), the major characteristics of the annual mean SST bias pattern are still the same, suggesting the linkage between cold bias in the Northern Hemisphere and warm bias in the Southern Oceans by the Atlantic meridional overturning circulation (AMOC). It is notable that the cold biases in the Indian monsoon region and Pacific cold tongue region in CMIP6 are much improved compared with CMIP5. However, warm bias in the tropical Pacific is strengthened in CMIP6. Fig. 1f shows the zonal mean of SST bias. Between the equator and 10°N and between 30°N and 50°N, the zonal mean bias of winter and spring switches signs in summer and autumn. In the high latitudes, it is clearly shown again that warm bias is located in the Southern Oceans and cold bias in the Northern Hemisphere.

Furthermore, the mean, standard deviation, correlation, root mean square error (RMSE) and trend of the global mean SST was examined. Both the mean and standard deviation of the multi-model ensemble mean (MMM) are larger than those of the observations (Fig. 2a and b). The majority of these 48 models are well correlated with observations (Fig. 2c and d). However, the majority of models underestimate the trend of climate change (Fig. 2e). For individual models, FGOALS-g3 (Model 24), FIO-ESM v2.0 (Model 25), IPSL-CM6A-LR-INCA (Model 36), IPSL-CM6A-LR (Model 35), and MPI-ESM-1-2-HR (Model 40) are in the top 5 in simulating the mean, standard deviation, correlation, RMSE, and trend (Fig. 2a–e, Table 1). However, IPSL-CM6A-LR-INCA overestimates the trend, with the trend in MPI-ESM-1-2-HR smaller than the observed trend (Fig. 2e). Both FGOALS-g3 and FIO-ESM v2.0 show high performance, but they only resolve medium resolution. The possible explanation can be related to their setup features. For example, FGOALS-g3 adopts a grid-point atmospheric model and involves improved parameterization of cloud microphysical processes (Li et al., 2020a; Li et al., 2020b). For FIO-ESM v2.0, the model considers the effects of nonbreaking wave mixing, and the effects of Stokes drift and sea spray droplets on sea surface fluxes, which involves the parameterization of SST diurnal variation (Bao et al., 2020; Song et al., 2020).

Similarly, the SSS bias was checked, and it was found that the spatial pattern of SSS bias is also consistent throughout the annual cycle with

https://doi.org/10.1016/j.dsr2.2022.105120
Received 25 April 2022; Received in revised form 20 May 2022; Accepted 23 May 2022
Available online 28 May 2022

Table 1
The models used in the analysis. The asterisk notes the two models that do not provide the SSS output.

No.	Model Name	Mean (°C) (Obs. 18.1775)		Detrended STD (°C) (Obs. 0.0922)		Trend (°C/decade) (Obs. 0.0639)		Correlation		RMSE (°C)		Mean Score	Total Rank
		value	rank	value	rank	value	Trend	value	Rank	value	Rank		
1	ACCESS-CM2	18.38	11	0.11	8	0.04	32	0.88	27	0.11	11	17.8	12
2	ACCESS-ESM1-5	19.00	39	0.16	45	0.04	31	0.89	33	0.14	39	37.4	44
3	AWI-CM-1-1-MR	17.93	14	0.12	16	0.07	4	0.85	12	0.14	13	11.8	7
4	AWI-ESM-1-1-LR	17.39	37	0.11	13	0.07	8	0.87	5	0.14	37	20.0	18
5	BCC-CSM2-MR	18.76	31	0.09	4	0.05	23	0.86	16	0.15	31	21.0	20
6	BCC-ESM1	18.90	35	0.13	25	0.02	43	0.85	41	0.15	35	35.8	42
7	CAMS-CSM1-0*	18.56	20	0.11	12	0.04	29	0.75	25	0.15	20	21.2	21
8	CAS-ESM2-0	18.48	17	0.15	43	0.02	47	0.69	47	0.20	17	34.2	38
9	CESM2	18.73	30	0.13	29	0.04	27	0.70	29	0.20	30	29.0	31
10	CESM2-FV2	18.85	33	0.15	39	0.03	39	0.85	42	0.24	34	37.4	45
11	CESM2-WACCM	18.62	25	0.14	35	0.05	24	0.81	31	0.25	25	28.0	29
12	CESM2-WACCM-FV2	19.00	40	0.14	34	0.02	42	0.86	40	0.27	40	39.2	46
13	CIESM	18.92	36	0.09	1	0.08	18	0.86	2	0.28	36	18.6	14
14	CMCC-CM2-HR4	18.97	38	0.10	6	0.07	7	0.85	8	0.29	38	19.4	16
15	CMCC-CM2-SR5	18.60	23	0.15	42	0.07	10	0.52	26	0.30	24	25.0	26
16	CMCC-ESM2	18.52	19	0.14	36	0.07	6	0.88	22	0.33	19	20.4	19
17	CanESM5	18.16	3	0.15	44	0.07	13	0.52	17	0.36	6	16.6	11
18	EC-Earth3	19.09	43	0.18	48	0.06	11	0.59	32	0.37	43	35.4	41
19	EC-Earth3-AerChem	19.10	44	0.18	47	0.04	33	0.84	39	0.37	44	41.4	47
20	EC-Earth3-CC	19.44	48	0.13	33	0.10	38	0.82	1	0.41	48	33.6	36
21	EC-Earth3-Veg	19.19	47	0.13	24	0.06	3	0.87	11	0.42	47	26.4	27
22	EC-Earth3-Veg-LR	19.05	41	0.12	18	0.05	25	0.68	24	0.43	41	29.8	33
23	FGOALS-f3-L	17.98	10	0.12	17	0.06	1	0.82	19	0.45	10	11.4	6
24	FGOALS-g3	18.17	1	0.11	9	0.06	9	0.82	7	0.45	1	5.4	1
25	FIO-ESM-2-0	18.10	6	0.11	10	0.06	2	0.75	9	0.47	4	6.2	2
26	GFDL-CM4	17.75	24	0.12	22	0.05	26	0.89	23	0.49	23	23.6	24
27	GFDL-ESM4	18.40	12	0.14	38	0.02	46	0.52	45	0.51	15	31.2	34
28	GISS-E2-1-G	18.86	34	0.13	32	0.03	36	0.57	35	0.55	33	34.0	37
29	GISS-E2-1-G-CC	18.81	32	0.12	21	0.06	12	0.68	21	0.57	32	23.6	25
30	GISS-E2-1-H	19.09	42	0.14	37	0.05	22	0.76	28	0.57	42	34.2	39
31	GISS-E2-2-H	17.63	29	0.12	23	0.03	40	0.86	37	0.59	29	31.6	35
32	ICON-ESM-LR	18.40	13	0.15	40	0.08	17	0.84	14	0.64	12	19.2	15
33	IITM-ESM	18.44	15	0.09	2	0.05	15	0.70	18	0.70	14	12.8	8
34	IPSL-CM5A2-INCA	17.89	16	0.13	30	0.09	30	0.59	6	0.70	16	19.6	17
35	IPSL-CM6A-LR	18.10	7	0.12	19	0.07	5	0.62	15	0.74	5	10.2	4
36	IPSL-CM6A-LR-INCA	18.13	4	0.11	14	0.08	19	0.90	4	0.75	2	8.6	3
37	MCM-UA-1-0	19.12	45	0.13	26	0.07	14	0.88	13	0.79	45	28.6	30
38	MIROC6	18.57	21	0.13	27	0.03	37	0.88	38	0.80	22	29.0	32
39	MPI-ESM-1-2-HAM	17.86	18	0.11	7	0.02	48	0.70	43	0.84	18	26.8	28
40	MPI-ESM1-2-HR	18.12	5	0.10	3	0.05	20	0.64	20	0.84	3	10.2	5
41	MPI-ESM1-2-LR	17.78	22	0.11	11	0.05	16	0.82	10	0.88	21	16.0	10
42	MRI-ESM2-0	18.20	2	0.10	5	0.03	34	0.80	30	0.93	7	15.6	9
43	NESM3	18.06	9	0.13	28	0.04	28	0.75	34	0.93	9	21.6	23
44	NorCPM1	17.70	27	0.07	15	0.05	21	0.65	3	0.94	26	18.4	13
45	NorESM2-LM	19.16	46	0.15	41	0.02	45	0.86	48	0.95	46	45.2	48
46	NorESM2-MM	18.64	26	0.17	46	0.03	41	0.50	46	1.01	27	37.2	43
47	SAM0-UNICON	18.07	8	0.12	20	0.03	35	0.87	36	1.02	8	21.4	22
48	TaiESM1*	18.69	28	0.13	31	0.02	44	0.90	44	1.27	28	35.0	40

significantly high salinity biases in the Bay of Bengal (1 PSU), the Atlantic Warm Pool region (1 PSU) and the Arctic (3 PSU) (Fig. 3a–e). This warm bias pattern is further presented by the zonal mean of SSS bias (Fig. 3f). In this overview of this special issue, a general picture of SST and SSS simulated in CMIP6 models is provided, rather than further investigate the mechanism that controls the biases pattern. In the next section, the papers collected in this special issue are briefly introduced.

2. Highlights of papers in this issue

The first paper in this issue investigates El Niño-Southern Oscillation (ENSO) phase-locking biases from the CMIP5 to CMIP6 models (Liao et al., 2021). The ENSO system is the most significant equatorial interannual climate variability pattern and has enormous global climate impacts. The ability to forecast ENSO accurately is crucially important to human livelihoods worldwide. ENSO is characterized by strong winter-peaking SST anomalies in the central-eastern tropical Pacific during the mature phase. However, the bias in simulating ENSO phase-locking behavior persists in climate models. In this study, the ENSO seasonal phase-locking behaviors simulated in 42 CMIP6 models are evaluated by comparing 43 CMIP5 models and observations. Only a few models (12 CMIP5 and 15 CMIP6) simulated ENSO with a majority proportion of winter-peaking events, which indicates that reasonable ENSO seasonal phase locking is still a challenge for state-of-the-art climate models. Furthermore, the seasonal cycle of the zonal SST gradient along the equator can explain approximately 24% and 27% of the variance in the ENSO phase locking for CMIP5 and CMIP6, respectively. In particular, the strengths of the zonal SST gradient in the central-eastern Pacific during boreal spring and autumn are crucial. The biases in simulating the seasonal changes in the zonal SST gradient influence the zonal advective feedback's strengths that respond to the anomalous SST of ENSO, therefore disturbing the simulation of ENSO phase locking. Improvement of the simulated ENSO phase locking should be realized by focusing on seasonal cycle of the zonal SST gradient.

Ding et al. (2021) focused on Ningaloo Niño simulated by two coupled models of the Flexible Global Ocean-Atmosphere-Land System model version (FGOALS3). Ningaloo Niño, an interannual SST warming

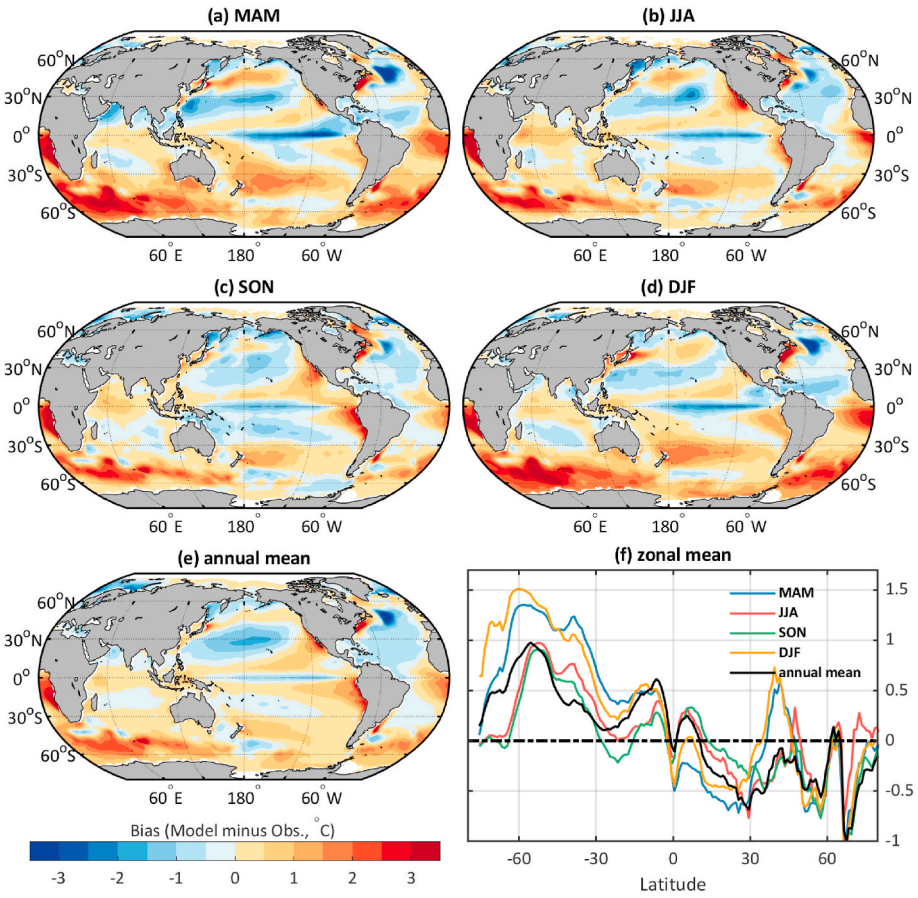

Fig. 1. Modelled SST ensemble mean bias of (a) spring, (b) summer, (c) autumn, (d) winter, (e) annual mean, and (f) zonal mean.

phenomenon off western Australia, has a significant impact on the regional ecosystem and arouses economic damage. Using two coupled models, FGOALS-g3 and FGOALS-f3-L, they evaluated their simulation ability for Ningaloo Niño. The results show that the two models can reproduce the basic characteristics of Ningaloo Niño well, including the spatial pattern and phase-locking feature. The amplitude of Ningaloo Niño is underestimated in FGOALS-g3 but is well duplicated in FGOALS-f3-L. The difference in cloud shortwave radiation-SST feedback between the two models is the key contributor to the different Ningaloo Niño amplitudes between the two models. A positive stratus cloud shortwave radiation-SST regime is exhibited in FGOALS-f3-L, which is similar to that operated in the observation, while FGOALS-g3 unsuccessfully simulates such a shortwave radiation-SST regime, which may be traced back to the model parameterization schemes in the atmospheric component of FGOALS-g3. In the observation, the development of Ningaloo Nino involves two different modes (local mode and nonlocal mode). Their results show that the two modes can be reproduced well in FGOALS-g3, whereas only one single mode (e.g., local mode) is manifested in FGOALS-f3-L. From the statistical perspective, both the observations and FGOALS-g3 show that there is a significant connection between tropical ENSO signals and Ningaloo Niño/Nina to some extent, while FGOALS-f3-L does not have such a significant statistical relationship. Thus, it is argued that the failure to represent the inter-basin connection in FGOALS-f3-L may be responsible for the absent nonlocal mode.

Qiu et al. (2021) evaluated and projected global marine heatwaves (MHWs) based on CMIP6 models. MHWs are extreme climatic events that last for days to months and can extend up to thousands of kilometers. MHWs cause substantial ecological, social, and economic impacts. While climate models are the key tool for studying and predicting MHWs, it continues to be challenging for climate models to accurately simulate MHWs. In this study, the authors evaluate 29 models from CMIP6 and 19 models from CMIP5 in terms of their capabilities to simulate MHWs by examining the spatial patterns and temporal variations. They estimate future changes until the end of the 21st century under three shared socioeconomic pathways (SSPs) (e.g., SSP126, SSP245, and SSP585). The results show that the CMIP6 ensemble mean is more skillful in capturing the features of MHWs than that of CMIP5. The biases of the CMIP6 models for the MHWs intensities are within ±0.5 °C over most of the oceans, except in the western boundary current regions and eastern tropical Pacific, where the modelled MHWs are up to 1.5 °C weaker than the observations. In comparison, the results from CMIP5 are greater than ±1.5 °C in most areas. Both the CMIP5 and CMIP6 models underestimate long-duration MHWs in the eastern tropical Pacific, where they are nearly 20 days shorter than the observations. In most areas, the CMIP5 models overestimate the MHWs durations (by over 25 days), while the biases of the CMIP6 models are within 10 days. The projected MHWs exhibit significant increases in intensity and duration and reach maximum intensities of 4 °C. The largest changes are projected to occur in the tropics, North Pacific, and North Atlantic. When comparing the shared socioeconomic pathways for the increasing trend of MHWs, the most extreme MHWs occur under SSP585, with their intensities nearly doubling and a near-permanent MHWs state occurring by the 2070s.

The fourth paper discussed the effects of a freshening trend on upper-ocean stratification over the central tropical Pacific and their representation by CMIP6 models (Li and Zheng, 2022). Along with global warming, the increasing trend in the freshwater flux (FWF) into the ocean in the central tropical Pacific (CP) is causing a freshening trend in seawater to reconstruct the upper oceans. In this work, the linear trend in stratification directly induced by the freshening trend is isolated by Argo data from 2005 to 2020, and a positive feedback process is

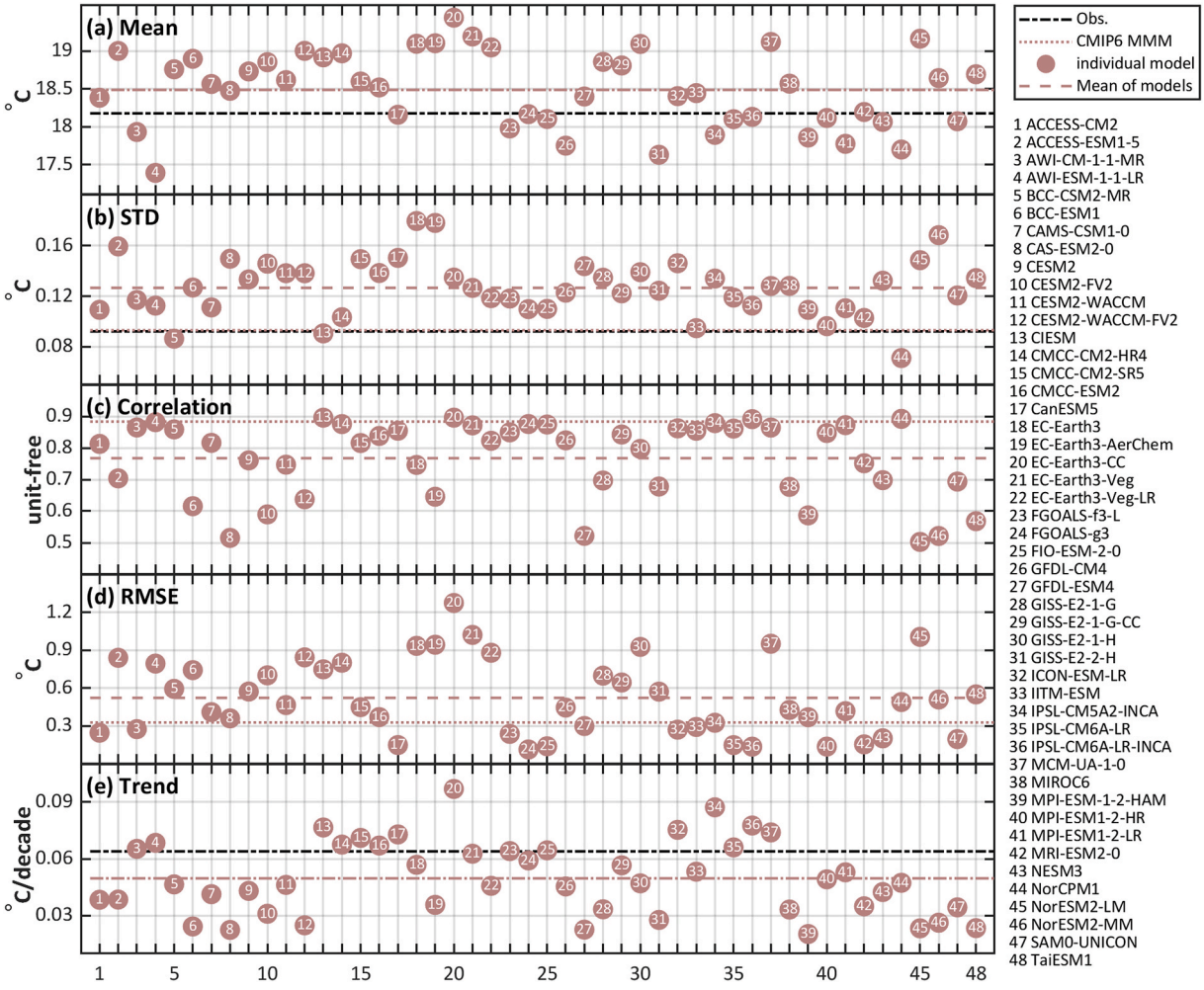

Fig. 2. Individual model and model ensemble mean of global averaged SST a) mean, b) standard deviation, c) correlation with observation, d) RMSE and e) trend.

proposed and verified by a 1-D model to understand how the freshening trend can modulate the temperature trend over the CP. The freshening trend in the mixed layer (ML) induced by the increasing FWF trend makes the stratification in the ML more stable by thickening the barrier layer (BL) and reducing the entrainment of subsurface cold water. Therefore, there is feedback on warming from FWF and salinity effects. Furthermore, 33 CMIP6 models were used to validate the model's ability to reproduce the physical process in which the freshening trend in the ocean induces a thicker BL. Seventy percent of the 33 models can reasonably simulate the freshening trend. Only 52% of the 33 models correctly reproduce the abovementioned physical process. Serious deviations are present in the simulation for the shoaling trend in the isothermal layer depth in the remaining models.

The fifth paper by Wang et al. (2022) studied the simulated sea levels during 1948–2009 in a global ocean-sea ice model for the Ocean Model Intercomparison Project (OMIP). This paper assessed the ability of the State Key Laboratory of Atmospheric Science and Geophysical Fluid Dynamics of the Institute of Atmospheric Physics (LASG/IAP) Climate System Ocean Model version 3 (LICOM3) to simulate sea levels. For the time series of global changes, most of the global mean steric sea level (SSL) changes were dominated by thermosteric sea level (TSSL) changes in the upper 700 m, with a relatively small contribution from halosteric sea level (HSSL). LICOM3 can reproduce the observed dynamic sea level (DSL) in most regions to reflect the spatial patterns of regional changes. Deviations between LICOM3 and observations were mainly concentrated in the western boundary current and the tropical eastern Pacific. The departure in the western boundary current was primarily related to the model resolution. LICOM3 could not depict DSL changes in the high latitudes where the mesoscale eddies were active. The excessive negative trend in the tropical eastern Pacific was mainly caused by the trend error in the Coordinated Ocean-ice Reference Experiment II (CORE-II) forcing products. For the sea level variability, the analysis results of different DSL periods showed that the LICOM3 model could simulate interannual and decadal variability and the satellite altimeter period trend. At least 50 years of data was used to separate the decadal variability and long-term trend. The decadal variability had no significant effect on the 50-year long-term trend change in the DSL in the tropical western Pacific. Analysis of sea level component contributions showed that the changes in global time series, spatial patterns, and sea level variability mainly resulted from the change in TSSL. The TSSL changes in the upper 700 m could roughly reflect the TSSL changes for the whole depth, except for the North Atlantic and the Southern Ocean. In the Atlantic, the contribution of HSSL was comparable to and compensated by TSSL. When compared with reanalysis, the simulation generated differences in the Southern Ocean and North Atlantic. The linear trend of TSSL simulated by LICOM3 was much stronger than that simulated by reanalysis. The deviation of the Southern Ocean may be related to the CORE-II forcing product. The lack of observations in the Southern Ocean led to the uncertainty of the CORE-II forcing product.

The last paper by Gong et al. (2022) focused on AMOC. AMOC is an integrated upper-cell circulation in the Atlantic Ocean, that is widely linked to global oceans and climate. Here, the authors conduct a statistical overview of the modelled AMOCs on the basis of historical set-ups in CMIP5 and CMIP6 simulations, including the modelled AMOC

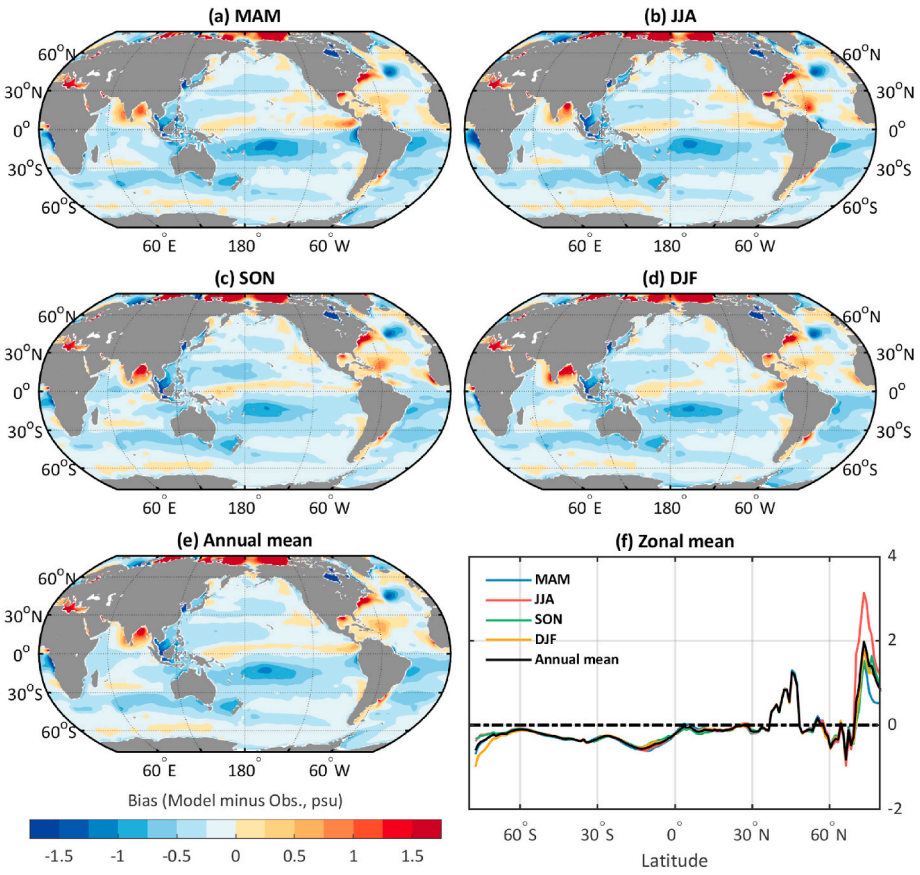

Fig. 3. Modelled SSS ensemble mean bias of (a) spring, (b) summer, (c) autumn, (d) winter, (e) annual mean, and (f) zonal mean.

strength, cell structure, long-term trend and variabilities on interannual, decadal and multi-decadal scales. These results showed that the CMIP6 multi-model averaged AMOC is relatively stronger than the CMIP5 result and further distinct from Rapid Climate Change Programme (RAPID) observations. In addition, there is no AMOC trend suggested by the CMIP6 results, different from a declining AMOC more commonly among CMIP5 simulations. Moreover, the multi-model averaged AMOC variabilities are comparable between CMIP5 and CMIP6 simulations on inter-annual, decadal and multi-decadal time scales, while the changes among models show discrepancies. Because AMOC acts as a comprehensive index for the background ocean and global climate, their statistical overview of the modelled AMOC in the CMIP5 and CMIP6 simulations provides essential information to understand the associated climatic process and analysis in this special issue.

The remarkable diversity of the papers in this special issue volume reports the progress of CMIP6 models from an ocean perspective. Although not able to cover all the major aspects of model evaluation, this special issue has provided crucial information for model development and research based on climate models.

CRediT author statement

All authors, at all stages, jointly conceived the study, discussed the results and implications, and commented on the manuscript. **Hailong Liu**: Writing-Original draft preparation, Conceptualization. **Zhenya Song**: Conceptualization, Visualization, Writing-Review & Editing, Supervision; **Xidong Wang**: Visualization, Validation, Writing-Review & Editing; **Vasu Misra**: Validation, Writing-Review & Editing.

Declaration of competing interest

The authors declare that they have no known competing financial interests or personal relationships that could have appeared to influence the work reported in this paper.

Acknowledgments

We thank the climate modeling groups for producing and making available their model output, the Earth System Grid Federation (ESGF) for archiving and providing access to data, and the multiple funding agencies which support CMIP and ESGF. All CMIP data are available from the ESGF at https://esgf-data.dkrz.de/search/cmip6-dkrz/. This work is supported by the National Natural Science Foundation of China (Grants 42022042, 41821004, and 41776019), Shanghai Typhoon Research Foundation, the China-Korea Cooperation Project on Northwest Pacific Marine Ecosystem Simulation under the Climate Change, and the CAS Interdisciplinary Innovation Team (JCTD-2020-12).

References

Bao, Y., Song, Z., Qiao, F., 2020. FIO-ESM version 2.0: model description and evaluation. J. Geophys. Res. Oceans 125, e2019JC016036. https://doi.org/10.1029/2019JC016036.

Ding, Y., Chen, L., Lin, P., Liu, H., Wang, R., 2021. Analysis of Ningaloo Niño simulated by two coupled models of FGOALS3. Deep Sea Res. Part II Top. Stud. Oceanogr. 194, 104988 https://doi.org/10.1016/j.dsr2.2021.104988 (this issue).

Gong, X., Liu, H., Wang, F., Heuzé, C., 2022. Of Atlantic Meridional Overturning Circulation in the CMIP6 Projects. Deep Sea Res. II (Under Review, this issue).

Huang, B., Thorne, P.W., Banzon, V.F., Boyer, T., Chepurin, G., Lawrimore, J.H., Menne, M.J., Smith, T.M., Vose, R.S., Zhang, H.-M., 2017. Extended reconstructed sea surface temperature, version 5 (ERSSTv5): upgrades, validations, and intercomparisons. J. Clim. 30, 8179–8205. https://doi.org/10.1175/JCLI-D-16-0836.1.

Li, K.-X., Zheng, F., 2022. Effects of a freshening trend on upper-ocean stratification over the central tropical Pacific and their representation by CMIP6 models. Deep Sea Res. II 195, 104999. https://doi.org/10.1016/j.dsr2.2021.104999 (this issue).

Li, L., Dong, L., Xie, J., Tang, Y., Xie, F., Guo, Z., Liu, H., Feng, T., Wang, Lu, Pu, Y., Sun, W., Xia, K., Liu, L., Xie, Z., Wang, Y., Wang, Longhuan, Shi, X., Jia, B., Liu, J.,

Wang, B., 2020a. The GAMIL3: model description and evaluation. J. Geophys. Res. Atmos. 125, e2020JD032574 https://doi.org/10.1029/2020JD032574.

Li, L., Yu, Y., Tang, Y., Lin, P., Xie, J., Song, M., Dong, L., Zhou, T., Liu, L., Wang, Lu, Pu, Y., Chen, X., Chen, L., Xie, Z., Liu, Hongbo, Zhang, L., Huang, X., Feng, T., Zheng, W., Xia, K., Liu, Hailong, Liu, J., Wang, Y., Wang, Longhuan, Jia, B., Xie, F., Wang, B., Zhao, S., Yu, Z., Zhao, B., Wei, J., 2020. The flexible global ocean-Atmosphere-Land system model grid-point version 3 (FGOALS-g3): description and evaluation. J. Adv. Model. Earth Syst. 12, e2019MS002012 https://doi.org/10.1029/2019MS002012.

Liao, H., Wang, C., Song, Z., 2021. ENSO phase-locking biases from the CMIP5 to CMIP6 models and a possible explanation. Deep Sea Res. II 189–190, 104943. https://doi.org/10.1016/j.dsr2.2021.104943 (this issue).

Qiu, Z., Qiao, F., Jang, C.J., Zhang, L., Song, Z., 2021. Evaluation and projection of global marine heatwaves based on CMIP6 models. Deep Sea Res. Part II Top. Stud. Oceanogr. 194, 104998 https://doi.org/10.1016/j.dsr2.2021.104998 (this issue).

Rayner, N.A., 2003. Global analyses of sea surface temperature, sea ice, and night marine air temperature since the late nineteenth century. J. Geophys. Res. 108, 4407. https://doi.org/10.1029/2002JD002670.

Song, Z., Bao, Y., Zhang, D., Shu, Q., Song, Y., Qiao, F.-L., 2020. Centuries of monthly and 3-hourly global ocean wave data for past, present, and future climate research. Sci. Data 7, 226. https://doi.org/10.1038/s41597-020-0566-8.

Wang, C., Zhang, L., Lee, S.-K., Wu, L., Mechoso, C.R., 2014. A global perspective on CMIP5 climate model biases. Nat. Clim. Change 4, 201–205. https://doi.org/10.1038/nclimate2118.

Wang, Y., Liu, H., Yu, Z., Lin, P., Ding, M., 2022. Simulated sea levels during 1948–2009 in a global ocean-sea ice model for OMIP. Deep Sea Res. II 199, 105082. https://doi.org/10.1016/j.dsr2.2022.105082 (this issue).

Zweng, M.M., Reagan, J., Seidov, D., Boyer, T., Locarnini, R., Garcia, H., Mishonov, A., Baranova, O.K., Paver, C., Smolyar, I., 2019. WORLD OCEAN ATLAS 2018 volume 2: salinity. In: Mishonov, A. (Ed.), NOAA Atlas NESDIS, vol. 82. Technical, p. 50.

Hailong Liu
School of Oceanography, Shanghai Jiao Tong University, Shanghai, China

Zhenya Song*
First Institute of Oceanography, and Key Laboratory of Marine Science and Numerical Modeling, Ministry of Natural Resources, Qingdao, China

Xidong Wang
College of Oceanography, Hohai University, China

Vasu Misra
Florida Climate Institute, Florida State University, Tallahassee, FL, USA

* Corresponding author. First Institute of Oceanography, and Key Laboratory of Marine Science and Numerical Modeling, Ministry of Natural Resources, Qingdao, China.
E-mail address: songroy@fio.org.cn (Z. Song).